Low-Voiding High-Reliability Lead-Free Solder Paste for Automotive Applications

Authored by: Jie Geng, Ph.D., and HongWen Zhang, Ph.D., Indium Corporation.

Abstract

A novel lead-free solder paste, DFHR, has been developed using Durafuse® technology. This technology demonstrates the combined merits of each constituent solder powder in the paste. DFHR is based on SnAgCu alloy system and contains bismuth (Bi), indium (In), and antimony (Sb). The paste melting temperature ranges from 205–221°C and can be processed with traditional 96.5Sn3Ag0.5Cu (SAC305) reflow profiles. Voiding performance was evaluated using Quad Flat No-Lead (QFN) components with OSP and ImSn surface finishes. The area percentage of voids for the thermal pad was less than 15%, being much lower than in SAC305. Thermal fatigue behavior was investigated under two thermal cycling profiles (1) -40°C/125°C and (2) -40°C/150°C with the same 10-minute dwell time at each extreme temperature. Thermal cycling tests were carried out using various components on daisy-chained test boards, including CABGA192, QFN (MLF68), and chip resistors (0603 and 1206). The degradation of solder alloys caused by thermal fatigue was evaluated with shear test and cross section investigation. DFHR voiding performance and thermal fatigue resistance improved dramatically compared to SAC305 and other high-reliability solder pastes.

Keywords: lead-free solder alloy, high reliability, low voiding, thermal fatigue reliability, shear test, thermal cycling.

Introduction

With automotive electronics booming, especially those in electrical vehicles (EV), more sensors and power moderators are increasingly required for electrical vehicles and self-driving cars. Lead-free tin-silver-copper (SnAgCu), solder alloys, such as Sn3.0Ag0.5Cu (SAC305) and Sn3.8Ag0.7Cu (SAC387), have become mainstream choices for surface mount technology (SMT) assembly in the electronics industry. These solders typically serve operation temperatures of 125°C and below, and they are widely used in computing, portable, and/or mobile electronics. Emerging automotive electronics demand service temperatures up to 150°C for devices used under the hood. Service temperatures below 125°C are still lean to compartment devices but desire longer service life than the mainstream SAC305 [1–4]. For such harsh electronics environments, the traditional binary or ternary lead-free Sn-rich solder alloys are not reliable enough to survive [1–6]. The higher the electronic device's operating temperature, the quicker the microstructure of the solder joint formed from the solder

DR. JIE GENG

Dr. Jie Geng, Research Metallurgist, is responsible for the development of novel lead-free high-reliability solder alloys for automotive applications. Jie also investigates the assembly process technologies in electronic packaging and interconnections.

Prior to joining Indium Corporation, Jie worked as a materials scientist. In that capacity, he gained extensive experience with materials selection, design, processing, and characterization, especially as it relates to processing-structure-property relationships in various materials including ultra-high temperature alloys, lightweight alloys (Al and Mg), magnetic materials, and ceramics.

Jie received his Ph.D. in Metallurgy from the University of Surrey in the United Kingdom. He is a Certified SMT Process Engineer and has published more than 30 journal articles.

email: jgeng@indium.com
Full biography:
www.indium.com/biographies

alloy coarsens and degrades. The recent development of high reliability, lead-free, and Sn-rich solder alloys demonstrates that additions of Sb, Bi, and In could improve the thermal fatigue resistance of solder joints in harsh thermal cycling or thermal shock conditions [7–11]. However, such solder alloys containing more than six elements exhibited poor voiding performance which is a common issue in the SMT assembly [12]. Voids in solder joints can lead to poor heat transfer, spot overheating, mechanical weaknesses, cracks in the joint, and general instability [12]. In this work, Durafuse® technology (mixing solder powder technology) was used to develop a novel Sn-Ag-Cu-Sb-Bi-In-Ni solder alloy (named as DFHR thereafter) with low voiding and high reliability [13–15]. It was compared to the control pastes SAC305 and 90.9Sn3.8Ag0.7Cu3Bi1.45Sb0.15Ni (denoted as SACBSbN).

DFHR Paste and Thermal Behavior

To achieve low voiding and high reliability, two different solder powders are mixed with flux into paste. One of the solder powders has a lower melting temperature than the other, comparable to or slightly lower than the melting temperature of traditional SnAgCu solder alloys, and the other solder powder has a melting temperature comparable to or higher than traditional SnAgCu solder alloys due to the addition of Sb [15]. The ratio of the two solder powders was tuned and optimized. DFHR was thus designed to exhibit both low voiding and high reliability. This paste can be reflowed with traditional SAC profile with peak temperature below 245°C. DFHR paste is based on SnAgCu alloy system with additions of Sb, Bi, In, and Ni.

The solder spheres formed by reflowing the mixture paste on ceramic coupons have been used to study the melting behavior by Differential Scanning Calorimetry (DSC). As shown in Figure 1, the melting of DFHR starts at 206°C and ends at 221°C. Its melting temperature is only 4° higher than SAC305 (217°C) allowing DFHR paste to be processed with traditional SAC profile without significant adaption. DFHR has the same melting temperature as SACBSbN (221°C), but starts melting earlier (206°C vs. 212°C).

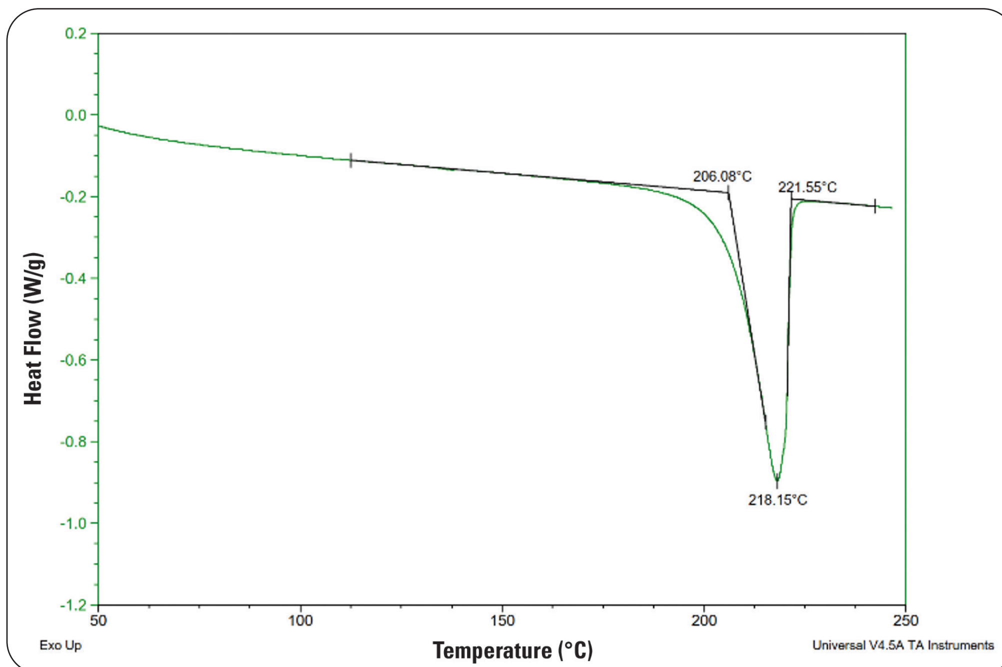

Figure 1. DSC curve of solder spheres formed by reflowing the mixture paste.

DR. HONGWEN ZHANG

Dr. HongWen Zhang is Manager of the Alloy Group in Indium Corporation's Research & Development Department. His focus is on the development of lead-free solder materials and the associated technologies for high-temperature and high-reliability applications. He also serves as a primary interface for existing products and processes with specific responsibility for expanding metallurgical innovation. Dr. Zhang and his team are responsible for using metallurgical insight to develop new products, implement improvements to existing processes and products, and measure results. Dr. Zhang was a co-inventor of the Durafuse® technology that is now used as an alternative way of designing lead-free solder paste for a variety of applications.

email: hzhang@indium.com
Full biography: www.indium.com/biographies

©2025 Indium Corporation

QFN Voiding Performance

To check the voiding performance, two test vehicles (TV) were used as shown in Figure 2: a) TV-a, small pad (5x5mm) QFN reflowed on Organic Solderability Preservative (OSP) surface finish, and b) TV-b, large pad (8x8mm) QFN reflowed on ImSn surface finish. The two types of QFN have the same body size of 10x10mm and pitch of 0.5mm (A-MLF68 10mm-.5mm-DC-Sn-TR-J). The print area is full coverage for TV-a and 3x3 window pane for TV-b. All three pastes were printed with 4mil-thick stencil and reflowed with profile shown in Figure 3. The peak reflow temperature is 239°C and the time above 221°C is 85 seconds. The temperature ramp rate between 180 and 220°C is 0.89 °C per second.

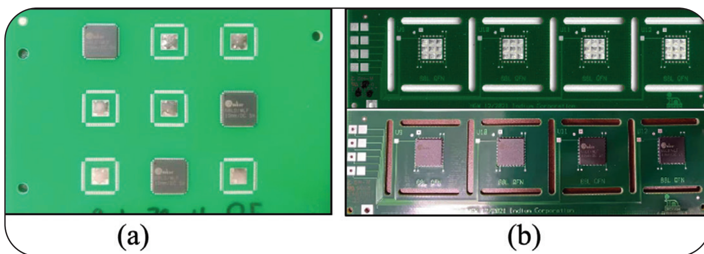

Figure 2. Test vehicles for voiding performance evaluation. a) TV-a, QFN reflowed on OSP surface finish b) TV-b, the top row showing the reflowed board without QFN (the printing pattern), and the bottom row showing the QFN reflowed on ImSn surface finish.

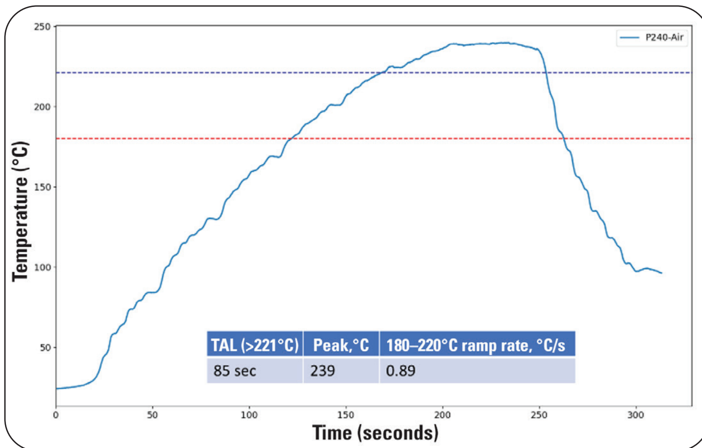

Figure 3. Reflow profile used for voiding performance test.

Figures 4 and 5 show the box plots of voiding data with individual points along with the typical X-ray images of three pastes. For both TV-a with small pad QFN and TV-b with large pad QFN, DFHR has the lowest average voiding among the three pastes. The average void area percentage in DFHR is below 10%, regardless of the pad size and surface finish. It is noted that the spread of data is much narrower with large pad which is printed with 3x3 window pane. X-ray images of SAC305 and SACBSbN in Figure 4 show that the void is large in size when printed with 5x5mm full area coverage. The size of the voids became smaller even with larger 8x8 mm pad but printed with 3x3 window pane, as evidenced in Figure 5. This indicates the design of stencil with window pane could help to improve the voiding performance.

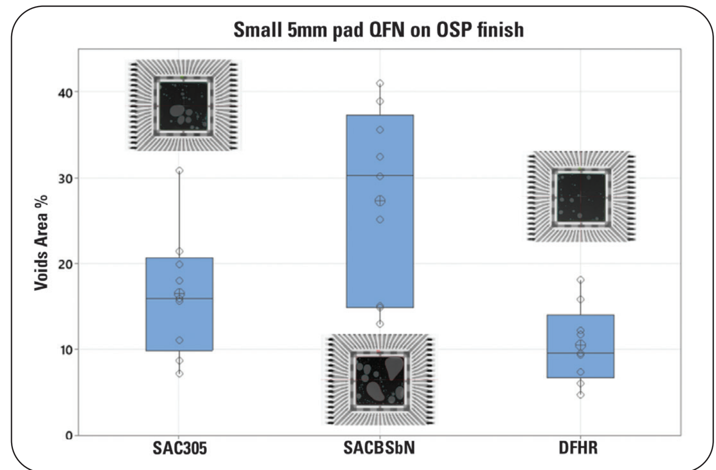

Figure 4. The voiding data and X-ray images for small 5mm pad QFN on OSP surface finish test board.

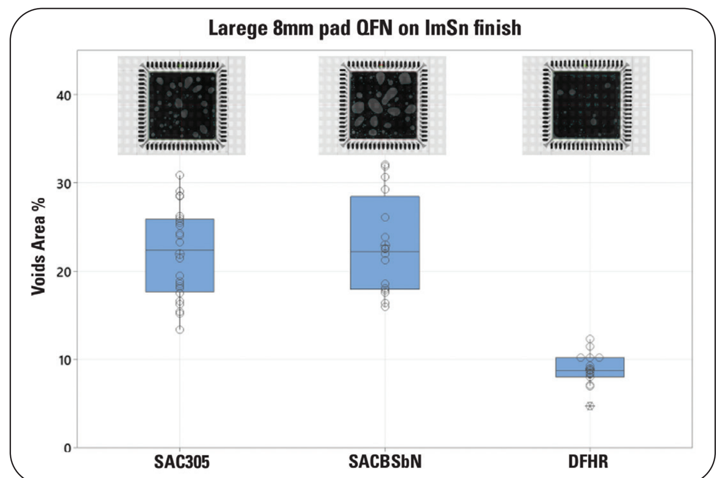

Figure 5. The voiding data and X-ray images for large 8mm pad QFN on ImSn surface finish test board.

©2025 Indium Corporation

Chip Resistor Thermal Cycling Test

Test Vehicle and Thermal Profiles

A daisy-chained resistor board – having both OSP and electroless nickel immersion gold (ENIG) surface finishes on the pads – was designed to test various chip resistors (Sn-plated terminals), including 0603 and 1206, as seen in Figure 6. The pad was solder-mask-defined. Temperature cycling profile -40°C to 125°C with 10 minutes dwell time was used for chip resistor testing. The cross section and shear test were done at intervals, 1,500, 2,000, 2500, 3,000, 4,000, and 4,650 cycles.

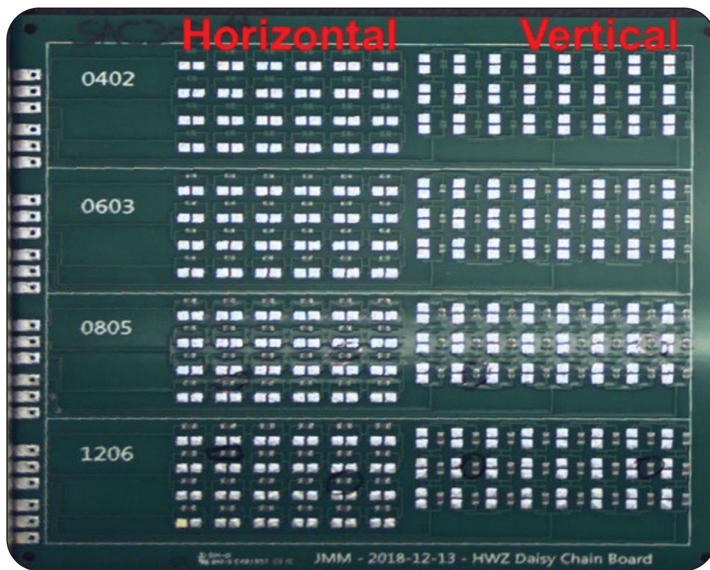

Figure 6. Chip resistor board for TCT.

Shear testing was done to check the bonding strength at different intervals up to 4,650 cycles under thermal cycle testing (TCT) -40°C/125°C. As shown in Figure 7, SAC305 and SACBSbN exhibited significant drop in shear strength compared to time zero. DFHR maintained its strength well within 3,000 cycles for R1206 and 4,000 cycles for R0603.

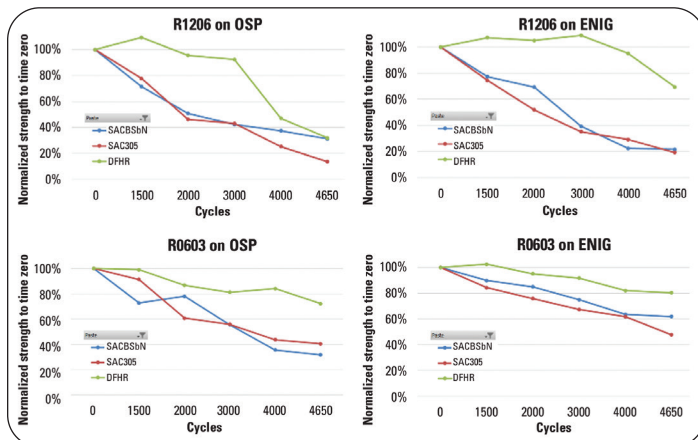

Figure 7. Shear strength of all types of chip resistors for three alloys at different intervals up to 4,650 cycles under TCT -40°C/125°C.

Figure 8 shows the optical images of cross sections of thermal cycled joints of all three alloys for 1206 chip resistors on the OSP and ENIG surface finishes. The micrographs show that cracks are in the bulk solder joints and they are formed by thermal fatigue. After 2,000 cycles, SAC305 and SACBSbN showed cracks under the resistor terminations while DFHR only exhibited the onset of cracks. Similar observation was made after 3,000 cycles. The OSP surface finish showed worse cracking than ENIG finish in the SAC305 and SACBSbN joints. Limited cracks were observed in the DFHR joints. The results indicate that DFHR has better crack resistance than SAC305 and SACBSbN under TCT -40°C/125°C.

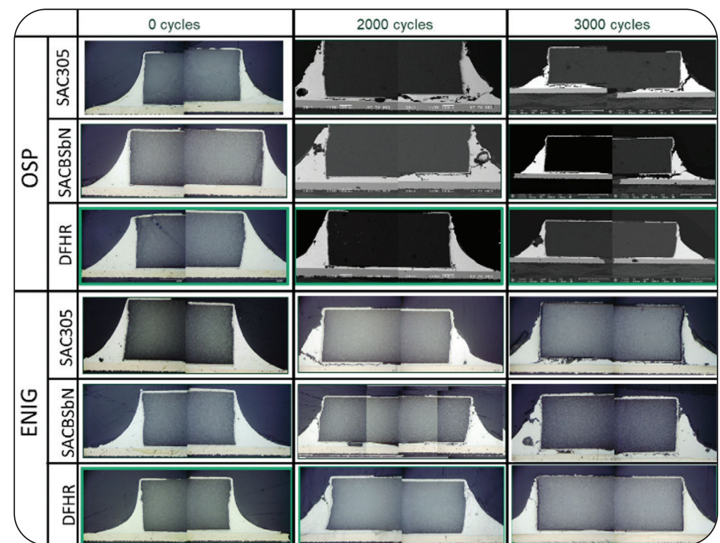

Figure 8. Optical images of cross sections of the 1206 chip resistors for all three alloys after 2,000 and 3,000 cycles under TCT -40°C/125°C.

Crack ratios were calculated from the sample cross sections. The crack ratio is the ratio of the manually measured crack length and the possible crack propagation length across the sample diameter. Generally, the lower the crack ratio is, the better the crack resistance of the material. Figure 9 shows

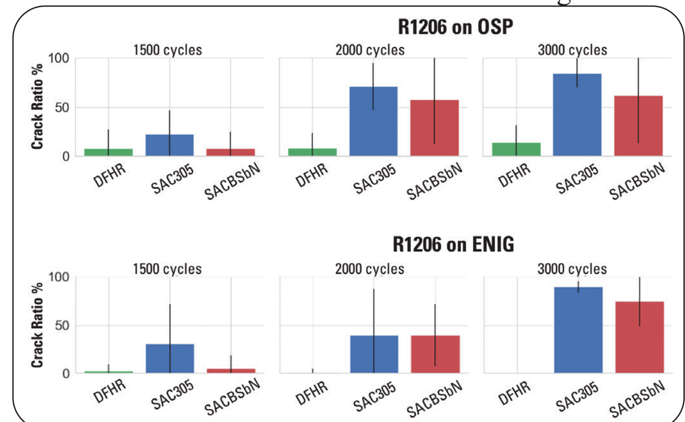

Figure 9. The crack ratios in 1206 resistors for three pastes at 1,500, 2,000, and 3,000 cycles under TCT -40°C/125°C.

©2025 Indium Corporation

the crack ratios in 1206 resistors after 1,500, 2,000, and 3,000 cycles under TCT -40°C/125°C. For each paste at each interval, six resistors were cross sectioned and examined for comparison. At 1,500 cycles, the SAC305 had the highest crack ratio among three pastes. The crack ratios in DFHR and SACBSbN were comparable. After 2,000 cycles, the rate of crack propagation in SACBSbN increased while that in DFHR was steady. At 2,000 cycles, the crack ratio in SACBSbN was above 50%, being much higher than that in DFHR which remained lower at 9% for 1206 resistor on OSP surface finish.

BGA and QFN Thermal Cycling Test

Test Vehicle and Thermal Profiles

A daisy-chained test board (Tg 170°C)—having both CABGA192 and QFN (MLF68—was designed with both OSP and ImSn surface finishes (Figure 10). The pad was solder-mask-defined. The progression of the thermal cycle test from CABGA192 and QFN was electrically monitored in situ. Two temperature cycling profiles were used in this work, 1) -40°C to 125°C, and 2) -40°C to 150°C. The dwell time for both profiles was set to 10 minutes.

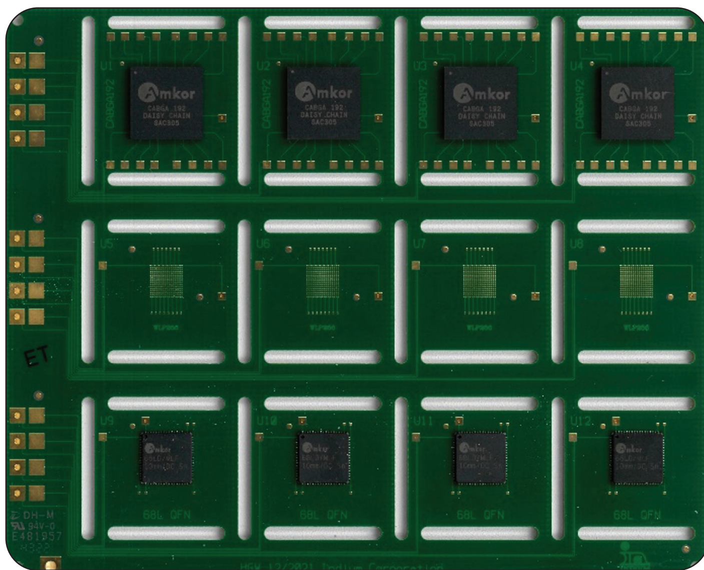

Figure 10. CABGA192 and QFN test board for TCT.

Thermal Cycling -40°C/125°C

TCT (-40°C/125°C) was performed for BGA-QFN test boards with both OSP and ImSn finishes, and the cross sections were examined at 2,000 and 3,000 cycles. The in-situ resistance monitoring has completed 4,400 cycles and is still ongoing, with the goal of reaching 63% failure for all three pastes.

Table 1 and Figure 11 show the failure information up to 4,400 cycles. There were 15 CABGA192s and 15 QFNs for each paste/finish before the thermal cycling test. As seen from

Table 1. Failure information of CABGA192 and QFN under TCT -40°C/125°C up to 4,400 cycles.

Component	Finish	Paste	Total	Failed	Failed, %	First	Last
BGA192	ImSn	SAC305	15	15	100	1379	3950
		DFHR	15	3	20	2425	4284
		SACBSbN	15	5	33.3	1877	4357
	OSP	SAC305	15	15	100	1498	3956
		DFHR	15	0	0	–	–
		SACBSbN	15	4	26.7	3968	4278
QFN	ImSn	SAC305	15	15	100	1748	3774
		DFHR	15	0	0	–	–
		SACBSbN	15	4	26.7	3087	4165
	OSP	SAC305	15	15	100	1741	3950
		DFHR	15	0	0	–	–
		SACBSbN	15	5	33.3	3950	3995

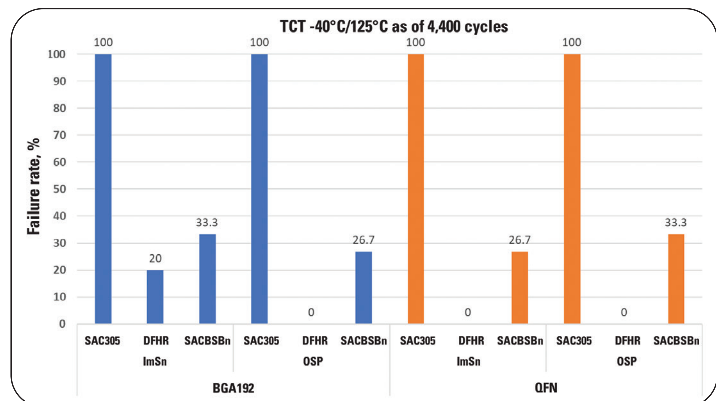

Figure 11. The failure rates of CABGA192 and QFN for all the three pastes under TCT -40°C/125°C as of 4,400 cycles.

Table 1 and Figure 11, all SAC305 joints of BGA and QFN failed after 4,000 cycles. DFHR only had three failures for CABGA192 on the ImSn surface finish and none for other cases. The failure rate of SACBSbN joints was about 30% for all the cases. The number of failures for DFHR and SACBSbN is not enough to get a meaningful Weibull analysis as of 4,400 cycles. The in situ monitoring is thus continued in order to do the Weibull analysis comparison. However, the cross sections were examined at 2,000 and 3,000 cycles to compare the thermal fatigue behavior.

The cross section of the CABGA192 was done at the first row as shown in Figure 12. There were 16 joints in this row, numbered B01 at the left to B16 at the right. The crack ratios at the both BGA chip side and the PCB board side were calculated according the schematic drawing shown in Figure 12.

©2025 Indium Corporation

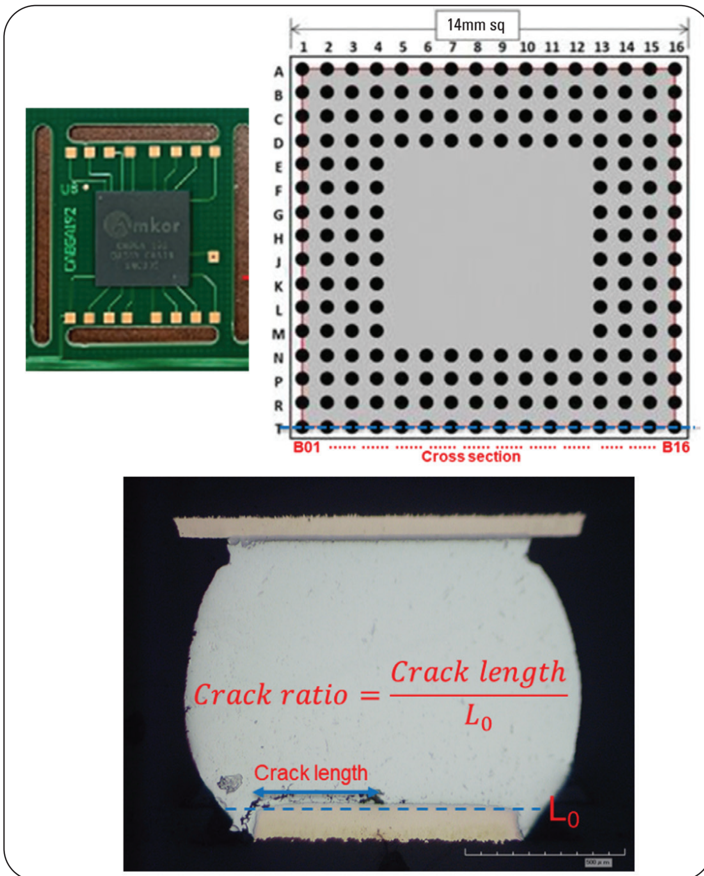

Figure 12. Schematic drawing shows the location of the cross sections examined for CABGA192 and the crack ratio calculation.

Figure 13 shows the cross sections of the corner joints (B01 and B16) from CABGA192 (on ImSn surface finish) after 2,000 cycles and the crack ratios of each individual joint measured from cross sections. SAC305 and SACBSbN exhibited severe cracking in the corner joints. The crack presented at the chip/component side in the SAC305 joint, but initiated at the PCB side in the SACBSbN joint. There was no obvious crack in DFHR joints. This observation is consistent with the data shown in Table 1 which shows the first failure of CABGA192 on ImSn surface finish for DFHR was at 2,425 cycles while the first failure of SAC305 and SACBSbN took place before 2,000 cycles.

Figure 14 shows the cross sections of the corner joints (B01 and B16) from CABGA192 (on ImSn surface finish) after 3,000 cycles and the crack ratios of each individual joint measured from cross sections. SAC305 and SACBSbN exhibited full cracks in the corner joints. The corner joint had nearly 60% crack ratio for DFHR.

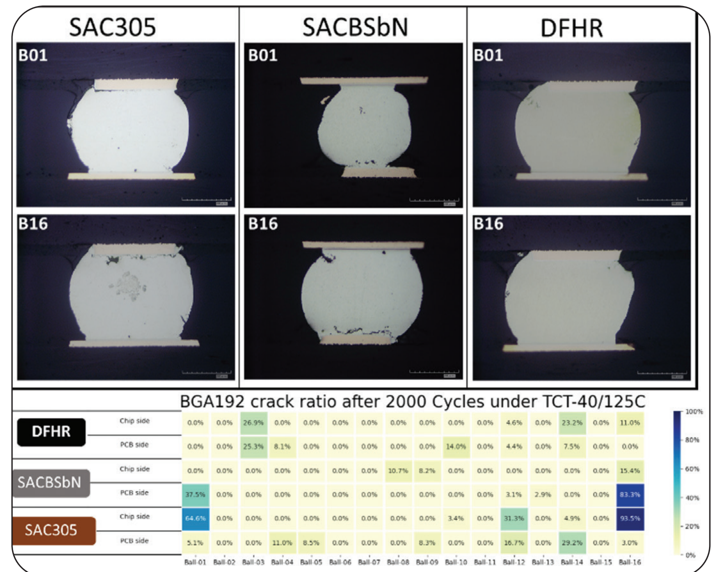

Figure 13. The cross sections of the corner joints from CABGA192 (on ImSn surface finish) and the crack ratio of each individual joint after 2,000 cycles under TCT -40°C/125°C.

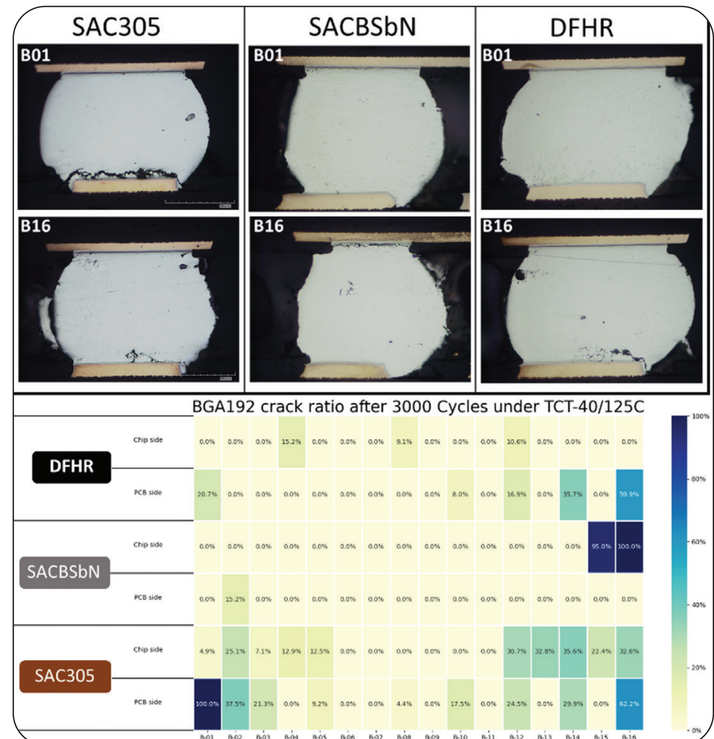

Figure 14. The cross sections of the corner joints from CABGA192 and the crack ratio of each individual joint after 3000 cycles under TCT -40°C/125°C.

©2025 Indium Corporation

Figure 15 is schematic showing the cross sections done for the leads of QFNs. The cross section contains 17 leads numbered as J1 to J17 (from left to right). Figures 16 and 17 show the optical images of joints J01 and J17 in the QFN (on ImSn surface finish) cross sections after 2,000 and 3,000 cycles under TCT -40°C/125°C. At 2,000 cycles, there were limited cracks in joints of all the three pastes, while after 3,000 cycles, the joints of SAC305 exhibited critical cracking, the joints being fully opened. SACBSbN also had fully opened joints. No fully opened joint was observed in trials using DFHR. The observations in cross section and crack ratio were consistent with the in-situ resistance monitoring data as shown in Table 1.

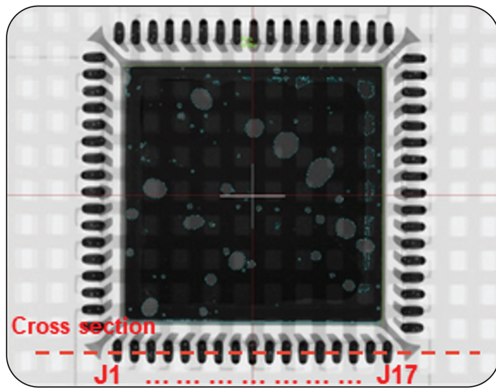

Figure 15. Schematic of cross-sectional location for the leads of QFNs.

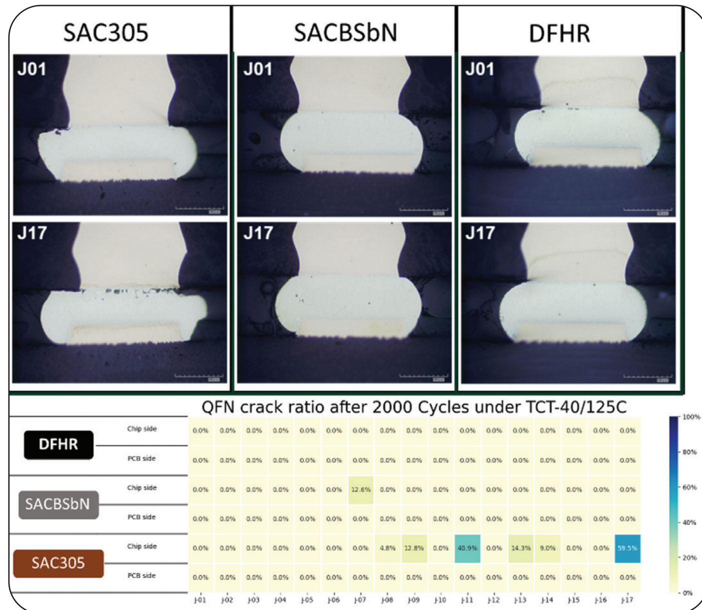

Figure 16. The optical images of corner joints and the crack ratios in the QFN (on ImSn surface finish) cross sections after 2,000 cycles under TCT -40°C/125°C.

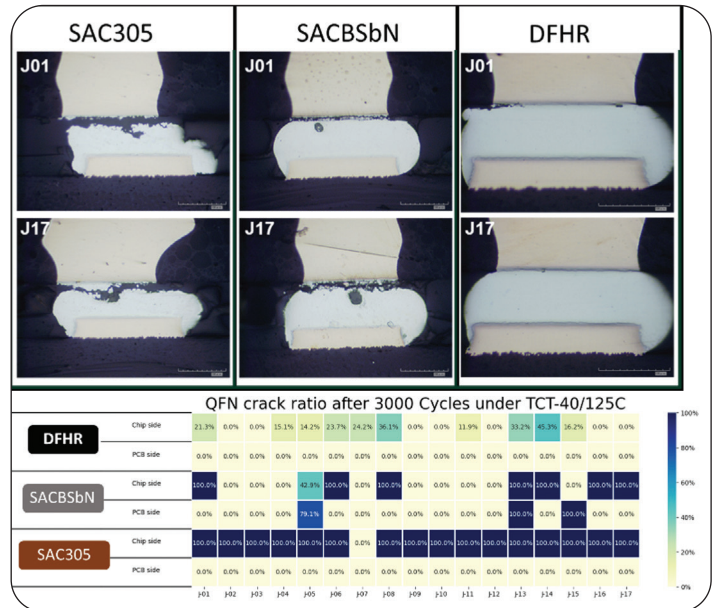

Figure 17. The optical images of corner joints and the crack ratios in the QFN (on ImSn surface finish) cross sections after 3000 cycles under TCT -40°C/125°C.

Thermal Cycling -40°C/150°C

TCT -40°C/150°C was performed for the same test boards (BGA-QFN) as shown in Figure 10. The thermal cycling has completed 3,000 cycles and is continuing until DFHR reaches 63% failure to allow for comparison under Weibull analysis.

Table 2 and Figure 18 show the failure information as of 3,000 cycles. SAC305 joints reached 100% failure after 2,311 cycles for all the CABGA192 and QFN. DFHR had the lowest failures among the three pastes. Noted that CABGA192 failed

Table 2. Failure information of CABGA192 and QFN under TCT -40°C/150°C as of 3,000 cycles.

Component	Finish	Paste	Total	Failed	Failed, %	First	Last
BGA192	ImSn	SAC305	16	16	100	284	2311
		DFHR	15	2	80	1020	2810
		SACBSbN	15	15	100	1166	2603
	OSP	SAC305	16	16	100	541	1805
		DFHR	15	11	73.3	608	2347
		SACBSbN	15	15	100	519	2647
QFN	ImSn	SAC305	16	16	100	1257	1888
		DFHR	15	3	20	2672	2780
		SACBSbN	15	13	86.7	1562	2699
	OSP	SAC305	16	16	26.7	1096	1999
		DFHR	15	3	20	2317	2727
		SACBSbN	13	7	53.8	2092	2674

©2025 Indium Corporation

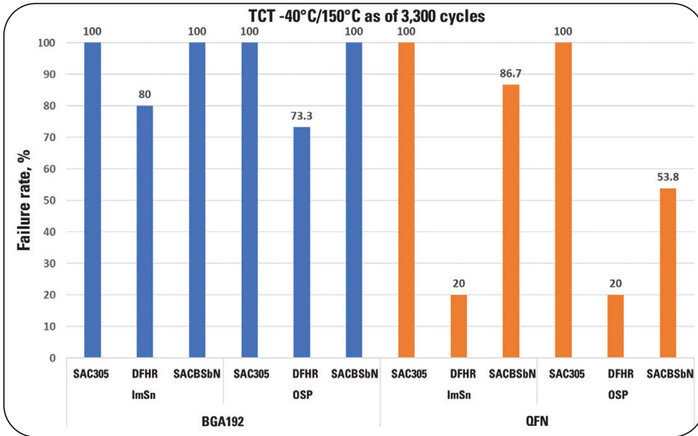

Figure 18. The failure rates of CABGA192 and QFN for all the three pastes under TCT -40°C/150°C as of 3,000 cycles.

earlier than QFN for all the pastes. CABGA192 had passed 63% failure for all the pastes. Thus, Weibull analysis (right-censored), as shown in Figure 19, was attempted to derive the characteristic lifetime for the pastes. The CABGA192 with SAC305 has characteristic lifetime about 1,000 cycles. While DFHR has more than 2,500 cycles for characteristic lifetime. SACBSbN performed secondly under TCT -40°C/150°C.

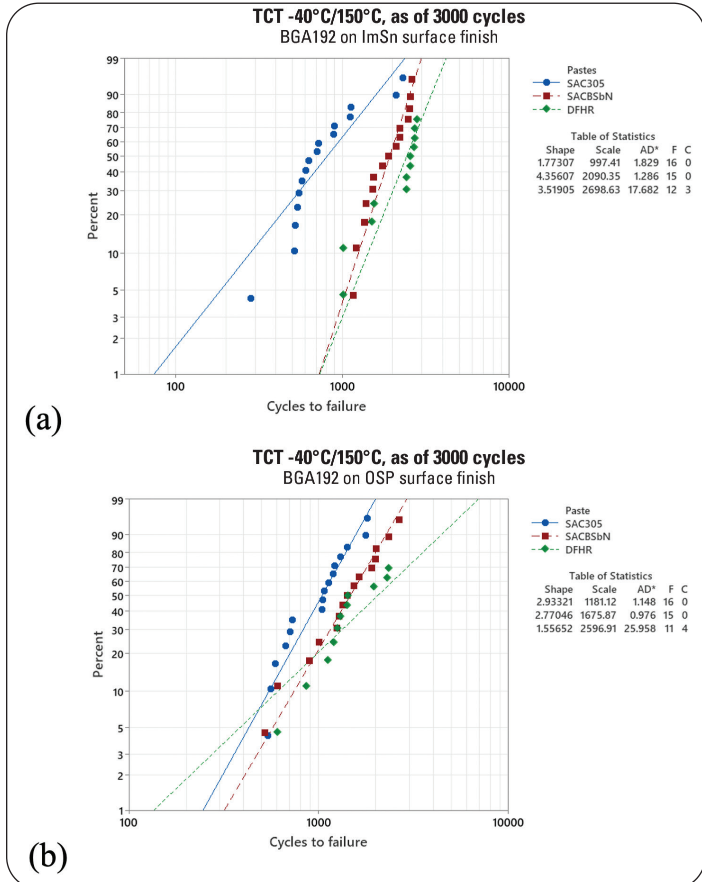

Figure 19. Weibull plots for CABGA192 on the (a) ImSn and (b) OSP surface finishes after 3000 cycles TCT -40°C/150°C.

Figure 20 shows the cross sections of CABGA192 on the ImSn surface finish after 2,000 and 3,000 cycles under TCT -40°C/150°C. At 2,000 cycles, no fully opened joint was observed in the DFHR or SACBSbN samples. SAC305 had one fully opened joint—B16 (Figure 14)—at the corner. The cracks initiated and propagated at both chip side and PCB side. At 3,000 cycles, both SAC305 and SACBSbN showed fully opened cracks. Though there was no fully opened crack in DFHR, the crack ratios reached 80% for the corner joints, B01 and B16 (Figure 14). The measured crack ratios match the trend shown in Table 2 and Figure 19.

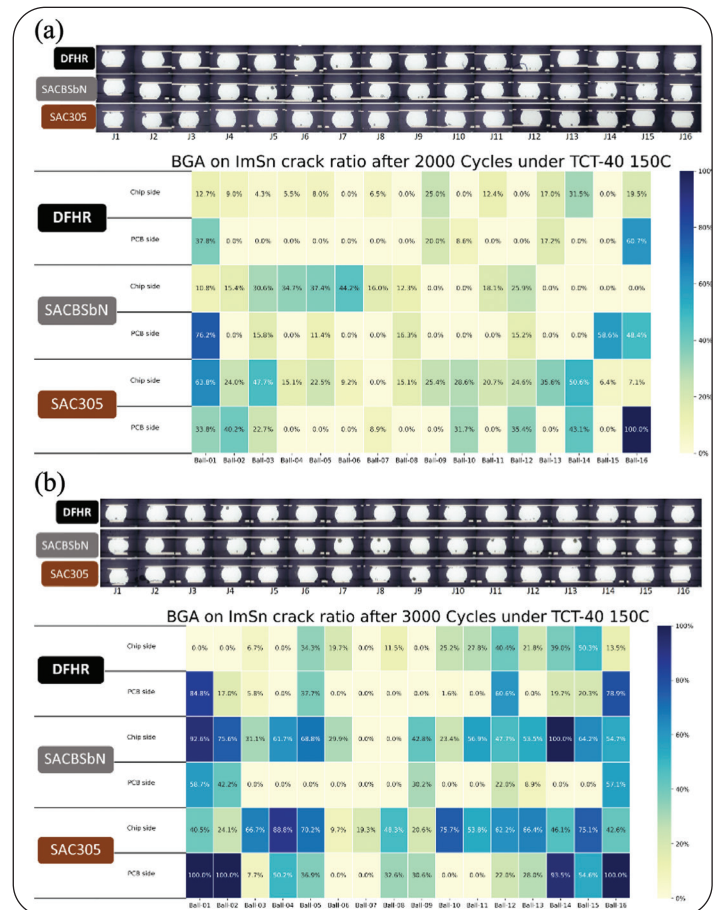

Figure 20. The optical images and the crack ratios in the CABGA192 (on ImSn surface finish) cross sections after (a) 2,000 and (b) 3,000 cycles under TCT -40°C/150°C.

©2025 Indium Corporation

Figure 21 shows the cross sections of QFN on the ImSn surface finish after 1,000 and 3,000 cycles under TCT -40°C/150°C. At 1,000 cycles, no obvious crack was observed in the joints of all the pastes. However, after 3,000 cycles, fully opened cracks were observed in all the pastes. The number of fully opened cracks in the SAC305 and SACBSbN were much more than that in DFHR. For SAC305, all the cracks were presented at the chip side.

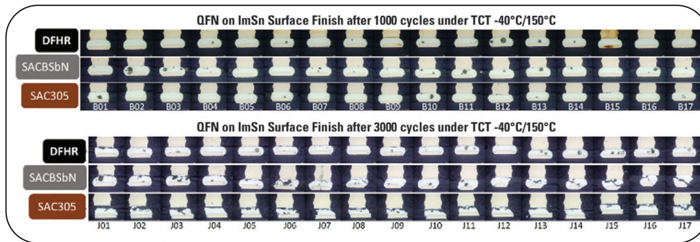

Figure 21. The optical images of the cross sections for QFN (on ImSn surface finish) after 1,000 and 3,000 cycles under TCT -40°C/150°C.

Conclusions

A novel lead-free solder paste, DFHR, has been developed using Durafuse® technology, i.e. mixing solder powder technology. DFHR is based on Sn-Ag-Cu alloy system and contains bismuth (Bi), indium (In), and antimony (Sb). The paste melting temperature ranges from 205–221°C and can be processed with traditional SAC305 reflow profiles. The area percentage of voids for the thermal pad of Quad Flat No-Lead (QFN) was less than 15%, being much lower than in SAC305 and SACBSbN. The joints formed with DFHR show improved thermal stability for chip resistors, CABGA192 and QFN than SAC305 and SACBSbN under TCTs -40°C/125°C and -40°C/150°C. In summary, both low-voiding and high thermal reliability could be achieved with DFHR lead-free solder paste.

References

1. Choudhury, P. et al. (May 2014). “New Developments in High-Reliability High-Temperature Pb-Free Alloys.” International Conference on Soldering & Reliability (ICSR), Toronto, Canada.
2. Ko, Y.H., Yoo, S.H., and Lee, C.W. (2010). “Evaluation on Reliability of High-Temperature Lead-Free Solder for Automotive Electronics.” Journal of the Microelectronics and Packaging Society. Vol. 17, No. 4. 35–40.
3. Miric, A.Z. (2010). “New Developments in High-Temperature, High-Performance Lead-Free Solder Alloys.” Balance. Vol. 90. 91-6.
4. Geng, J., Zhang, H., Mutuku, F., and Lee, N.C. (September 2018). “Novel Solder Alloy: Wide Service Temperature Capability for Automotive Applications.” IEEE Power Electronics Magazine. Vol. 5, No. 3. 56–62.
5. Coyle, R., Johnson, C., Hillman, D., Pearson, T., Osterman, M., Smetana, J., Howell, K., Zhang, H., Silk, J., Geng, J., Daily, D., Arfaei, B., Pandher, R., Delhaise, A., Longgood, S., and Kleyner, A. (2020). “Enhancing Thermal Fatigue Reliability of Pb-Free Solder Alloys with Additions of Bismuth and Antimony.” Proceedings of SMTA International. 339–354.
6. Henshall, G., Bath, J., Sethuraman, S., Geiger, D., Syed, A., Lee, M.J., Newman, K., Hu, L., Hyun Kim, D, Xie, Weidong, Eagar, W., and Waldvogel, J. (2009). “Comparison of Thermal Fatigue Performance of SAC105 (Sn-1.0Ag-0.5Cu), Sn-3.5Ag, and SAC305 (Sn-3.0Ag-0.5Cu) BGA Components with SAC305 Solder Paste.” Proceedings APEX. S05-03.
7. Arfaei, B., Mutuku, F.M., Coyle, R., and Cotts, E. (2016). “Influence of Micro-Alloying Elements on Reliability of SnAgCu Solder Joints.” SMTA Journal. Vol. 29, Issue 2.
8. Zhao, J., Qi, L., Wang, X.M., and Wang, L. (2004). “Influence of Bi on Microstructures Evolution and Mechanical Properties in SnAgCu Lead-Free Solder.” Journal of Alloys and Compounds. 375(1). 196–201.
9. Reeve, K.N., Holaday, J.R., Choquette, S.M., Anderson, I.E., and Handwerker, C.A. (2016). “Advances in Pb-Free Solder Microstructure Control and Interconnect Design.” Journal of Phase Equilibria and Diffusion. 37(4). 369–386.
10. Kang, S.K. (2012). “Effects of Minor Alloying Additions on the Properties and Reliability of Pb-Free Solders and Joints.” Lead-Free Solders: Materials Reliability for Electronics. John Wiley & Sons Ltd. 119–59.
11. Coyle, R., Read, P., McCormick, H., Popowich, R., and Fleming, D. (January-March 2011). “The Influence of Alloy Composition and Temperature Cycling Dwell Time on the Reliability of a Quad Flat No Lead (QFN) Package.” Journal of SMTA. Vol. 25, Issue 1. 28–34.
12. Lentz, T., Bixenman M. (2022). “Creation of a Novel Pb-Free Water-Soluble Solder Paste that Improves Reliability Through Low–Voiding and Ease of Washability.” Proceedings of SMTA International. 650–659.
13. Zhang, H.W., Lytwynec S., Wang, H.G., Geng, J., Mutuku, F.M. and Lee, N.C. (2023). “Lead-free Solder Paste with Mixed Solder Powders for High-Temperature Applications.” US Patent No. 11738411B2.
14. Zhang, H.W., Chen, F., Mutuku, F.M., Geng, J. and Lee, N.C. (2023). “Low-Temperature Melting and Mid-Temperature Melting Lead-Free Solder Paste with Mixed Solder Alloy Powders.” US Patent No. 11712762B2.
15. Geng, J. and Zhang, H.W. (2022). “High-Reliability Lead-Free Solder Pastes with Mixed Solder Alloy Powders.” US Patent No. 20220395936A1.

First presented at SMTAI 2023, Minneapolis, Minn., USA., October 9–12, 2023.

©2025 Indium Corporation